Asian Journal of Chemistry; Vol. 33, No. 10 (2021), 2439-2445

ASIAN JOURNAL OF CHEMISTRY

https://doi.org/10.14233/ajchem.2021.23185

Fabrication of Vanadium Doped Zinc Oxide Thin Film to Enhance the Optical, Magnetic and Electrical Properties using Electrospray Technique

M.H. Haja Sheriff[1], S. Murugan[1], R. Ashok Kumar[2] and A. Manivasaham[3,*]

[1]Department of Physics, A.V.C. College (Autonomous) (Affiliated to Bharathidasan University, Triuchirappalli), Mannampandal-609305, India
[2]Department of Physics, Vandayar Engineering College, Thanjavur-613501, India
[3]School of Physics, Madurai Kamaraj University, Madurai-625021, India

*Corresponding author: E-mail: maanivasahham@gmail.com

Received: 28 February 2021; *Accepted*: 6 August 2021; *Published online*: 20 September 2021; AJC-20518

Vanadium doped zinc oxide was deposited using a homemade electrospray technique. The structural, optical, magnetic, surface morphology and electrical studies were carried out using XRD, UV-vis-NIR spectroscopy, HRSEM, AFM, photoluminescence, VSM and Hall effect, respectively. The XRD results revealed that the addition of vanadium(V) does not affect hexagonal wurtzite structure in the films. Photoluminescence study implies the increase of oxygen vacancy on surface of the samples and the hexagonal plates like grains are found on the film surface and formation of cluster as doping percentage increases. Hall effect shows the remarkable improvement in carrier concentration, resistivity and mobility. The sheet resistance decreases to 59.5×10^2 Ω/^{2} for 4 at% of vanadium. All the samples achieved the transmittance above 80% in the visible region and optical band gap increases. The magnetic study shows that the enhancement of paramagnetic property and the study on the performances of the samples over the light intensity shows, the enhancement in the rate of decreases in resistance, which is higher than the undoped sample ware discussed.

Keywords: Thin films, Electrospray, Light intensity effect, Paramagnetic property, Doped zinc oxide film.

INTRODUCTION

In last two decades, the rapid development in the field of opto-electronics is associated with the requirement of user-friendly, eco-friendly, reduction in size and low cost material. Zinc oxide is one of such material and easily available in nature. Zinc oxide (ZnO) attracted the researchers as a flexible and appropriate material for their application, because of its wide band gap, high transparency, cheap, easy fabrication and high refractive index [1,2]. It finds large number of applications in the field of nanotechnology as a promising candidate for transparent conducting oxide (TCO), gas sensors, solar cells, surface acoustical wave guides, piezoelectric materials and heat sensing mirrors [3].

ZnO is non-toxic in nature, thermally and chemically stable and it has exciton binding energy (60 meV) and direct band gap [4], suitable for accepting structural and surface morphological changes on it. ZnO exhibits n-type semi conductivity due to its off stoichiometry [5]. This creates oxygen vacancy and zinc interstitials defects in its lattice and also creates shallow donor states within the forbidden energy gap [6]. This defects are large in number that increases the surface to volume ratio and provide an easy way for the interstitial and substitution of ions into its lattice plane [7]. Due to its acceptability nature, the researchers are trying with new and different types of elements for doping. ZnO acts as paramagnetic material at room temperature, it has larger ionic radius that makes easy to alter the magnetic property by adding suitable anions or cationic atoms. Addition of dopend will also modify the vacancies and lattice defects in ZnO structure that creates large changes in its magnetic property.

Fabrication of ZnO thin films involves many methods and attempts were made to synthesize thin films by simple and cost effective. These include chemical vapour deposition method [8], screen printing technique [9], RF magnetron sputtering [10], pulsed laser deposition [11], spray pyrolysis [12] and spin coating [13]. Among this methods, the modified spray pyrolysis as a homemade fully automated electrospray has been used to prepare ZnO thin films.

To improve the physical properties of ZnO thin film doping with metals and non-metals are essential. Researchers used some of the transition metal ions like Ta, Co, Ni, Fe, Cu, Mg, Sn, Mo, Cr, Mn as dopants to modify the electrical and surface morphology of ZnO [14]. In this work, vanadium(V) is chosen as a dopant and to study the magnetic, electrical and optical properties of V doped ZnO thin film.

EXPERIMENTAL

In this work, vanadium(V) doped ZnO samples were fabricated using fully automated homemade electrospray technique and coated over the glass substrate. To obtain 0.1 M and 50 mL precursor solution, zinc acetate dihydrate was dissolved with acetic acid, methanol and doubly deionized water in the ratio 1:2:7. For doping, vanadium(V) chloride was added with the precursor solution and the doping percentage of vanadium were 0, 2, 4 and 6 at%. The precursor solution was filled in the funnel shaped height adjustable reservoir. The substrate (Microscopic glass slides Lab. Tech. Medico (P) Ltd., India) of area 2.5 cm × 7.5 cm was fixed in vertical hot plate as shown in Fig. 1. The glass substrates were cleaned using HCl for 20 min, acetone for 10 min and by ultrasonic cleaner for 25 min (Supersonics, India) to remove the organic substance and moisture present if any on the surface of the glass substrate.

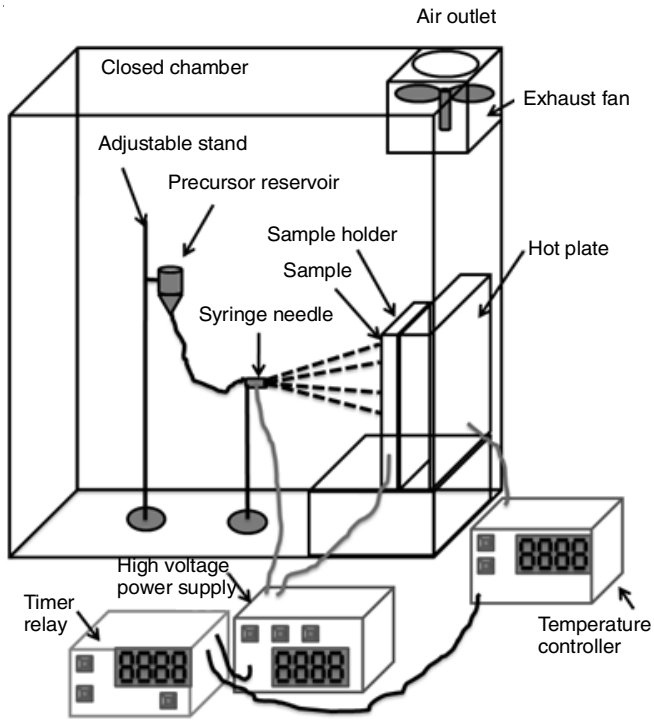

Fig. 1. Schematic diagram of the electrospray technique used to prepare as deposited and vanadium doped zinc tin oxide thin films

General procedure: The homemade electrospray consists of a syringe needle with the diameter 0.6 mm was attached to the reservoir through a tube and flow rate controller was used to control the precursor flow to get 0.002 mL/min at the needle tip. The needle and substrate surface distance was 8 cm as shown in Fig. 1. A high voltage (± 9.45 kV) was applied between needle and hot-plate to attract precursor solution towards substrate. The high voltage was adjusted so as to get cloud followed by Taylor cone and jet and the voltage was adjusted so that the mist reaches the hot substrate properly [15]. To get 500 nm thickness thin films, different volume of precursor solution was sprayed and found that 15 mL of precursor solution was suitable for the thickness. The thickness of all the samples was verified using weight gain method and profilometer measurement. A timer was used to connect high voltage power supply, relay and hot plate. The timer was used to power on the high voltage and power off the hot plate and *vice-versa*. Relay was connected to hot plate and syringe needle for grounding the charge present in it, as soon as high voltage was cut off. Distance between the syringe needle and substrate was adjusted to get precursor to form mist and decomposes at surface of the substrate. To conform the reproducibility at 360 ºC, four sets of V:ZnO thin film samples were deposited and the experiment were repeated for five times. It was found that the optimal time of deposition for each sample was about 45 min, which includes the spray intervals (10 s) and spray time (5 s) for each cycle.

Detection method: X-Ray diffractometer (PAN analytical-PW 340/60 X' Pert PRO) with X-ray (Cu*K*α) of wavelength 1.5406 Å used to study the structural properties of the prepared ZnO thin films. UV-vis NIR double beam spectrophotometer (LAMBDA-35) was used to study the optical transmittance with the wavelength range 300 to 1100 nm. The HRSEM images were obtained from scanning electron microscope (HITACHI S-3000 H). The profilometer was used to find thickness of the films by stylus technique (profilometer: Surf Test SJ-301) at four different areas on the surface of the thin film and the average thickness found to be around 500 nm and the weight gain method was also used to find the thickness. Four point probe technique with Vander Paw configuration (Ecopia-HMS3000) used to measure electrical resistivity of the films. Magnetic study was made using a vibrating sample magnetometer (VSM 7410). Light intensity response properties were studied using a Lux meter (L × 101A-HTCTM) and high range precession multimeter.

Light intensity effect study: A homemade experiment setup as shown in Fig. 2 was used to study the change in resistance towards the light intensity falls on the sample. It has a light source, sample holder, high range precession multimeter, light sensor, light intensity controller and Lux meter. Light intensity controller used to control the 1000 watts light source and an exhaust fan was used to remove the heat generated by the light. A transparent glass was placed in front of the light to prevent heating radiation effect over the sample. The distance between the sample holder and glass plate was about 40 cm. The sample holder was placed in front of the light source facing each other as shown in Fig. 2. Sample holder was connected to high range precession multimeter and the light source to Lux meter. Lux is used to measure the light intensity that falls on the sensor surface and this arrangement was placed inside an enclosed chamber.

RESULTS AND DISCUSSION

Structural studies: The XRD patterns of V doped ZnO thin films are shown in Fig. 3. All the observed peaks are matched exactly with the JCPDS card no. 36-1451 [16]. Results show

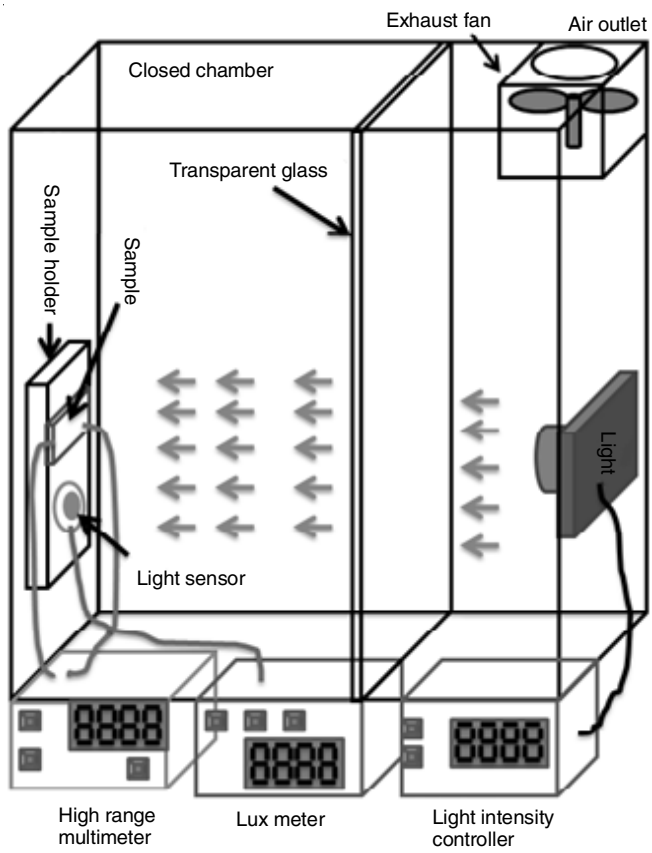

Fig. 2. Schematic diagram used to study the light intensity effect on resistance

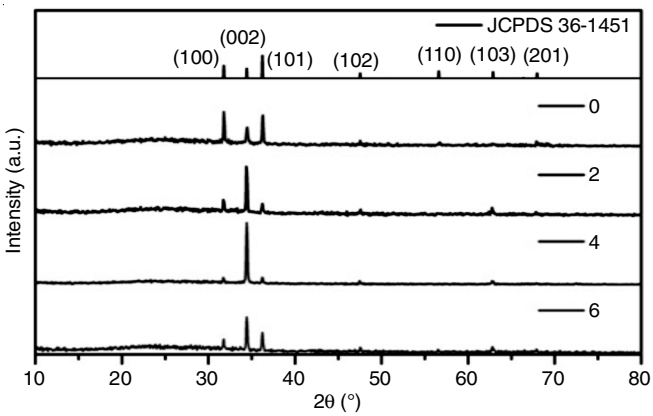

Fig. 3. XRD patterns of undoped and vanadium doped zinc oxide samples

that all the samples are having single phase with polycrystalline hexagonal wurtzite structure of ZnO. The preferential orientation of undoped film lies along (101) plane and for V doped ZnO films lies along (002) plane. This reorientation effect is due to incorporation of vanadium into ZnO lattice and surface energy required to grow along (002) plane is much smaller than the energy required to grow along (101) plane [17].

Since there is no secondary peaks corresponding to the dopant V in the XRD results, that indicates the purity of the ZnO:V samples. The incorporation of V^{5+} ions occupy either the regular Zn^{2+} sites in the lattice plane or segregate out to the non-crystalline region towards grain boundaries [18]. It has been found that the as-doping level increases the peak intensity increases along (002) plane, whereas the peak intensity of (101) plane decreases. This indicates the doping element V induces the reorientation of the crystallites along (002) plane. There is a small shift of (002) peak towards higher degree is observed in the doped films because of substitution of V^{5+} ions (ionic radius 72 Å) into the Zn^{2+} sites (ionic radius 74 Å). The shift in peak becomes the supporting evidence for the incorporation of the V into the ZnO lattice. It is also observed that substitution of smaller ions into a larger ionic lattice plane, the inter-planar distance (d) decreases, resulting in an increase of 2θ angles, from the Bragg's equation $2d \sin\theta = n\lambda$ [19]. The lattice constants 'a' and 'c' and crystallite size (D) are obtained using the following relations [20].

$$D = \frac{k\lambda}{\beta\cos\theta} \tag{1}$$

$$\frac{1}{d^2} = \left(\frac{4}{3a^2}\right)(h^+ + hk + k^2) + \frac{l^2}{c^2} \tag{2}$$

$$\delta = \frac{1}{D^2} \tag{3}$$

where k = 0.9 is the shape factor, λ is the wavelength of the Cu*K*α radiation (1.5406 Å) used, the full width at half-maximum (FWHM) is denoted as β, θ represent the Bragg's diffraction angle, Miller indices of the lattice planes were represented as (*h k l*) and d as the inter planar spacing. From the above equations, the crystallites size and lattice constants were calculated and observed that the values get decreased as V doping level increases (Table-1). The decrease in crystallite size and lattice parameters supported the evidence to the incorporation of V^{5+} ions into Zn^{2+} ionic lattices. The decreases in lattices constant are observed up to 4 at% of vanadium and for 6 at% the lattice constants starts increasing. For 6 at% sample, the crystallite size increases and it is also observed from XRD peaks intensity of 6 at% sample is lesser than that of 4 at%, which is due to reorientation effect of ZnO [21].

Optical studies: The optical property of undoped and V doped ZnO thin films were determined from the transmission spectra is shown in Fig. 4a. The transmittance was measured in the visible region ranges from 350 to 800 nm and it is around

TABLE-1
STRUCTURAL PARAMETERS OF UNDOPED AND V DOPED ZINC OXIDE THIN FILMS

ZnO samples (V, at%)	Preferential orientation plane (hkl)	Lattice constants (Å)			D (nm)	Strain	Dislocation density δ ($\times 10^{14}$ lines/m^2)
		d	a	c			
0	101	2.477	3.2496	5.6378	56	1.082	3.18
2	002	2.463	3.2432	5.6337	52	1.088	4.00
4	002	2.406	3.2397	5.6282	48	1.098	5.66
6	002	2.497	3.2456	5.6400	54	1.083	3.07

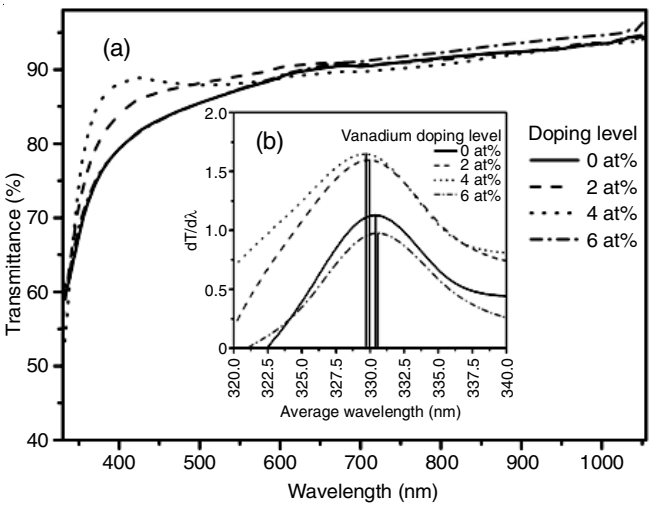

Fig. 4. (a) Transmittance spectra of V:ZnO samples (b) Optical band gap of V:ZnO thin films

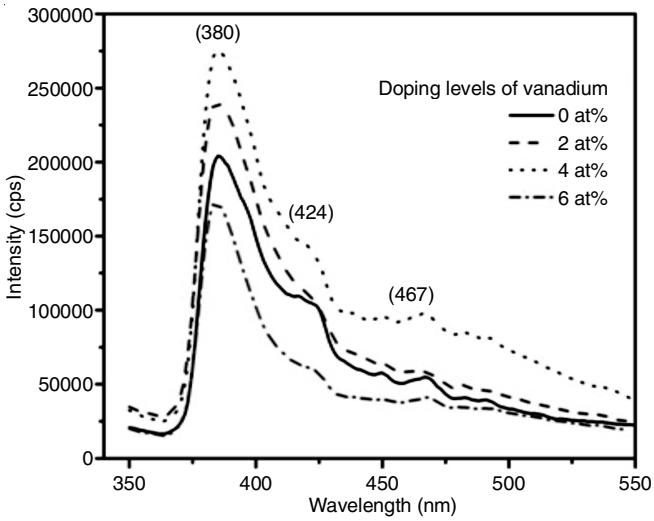

Fig. 5. PL spectra of as deposited and vanadium doped zinc oxide thin film samples

80%. The sharp absorption edge was found at 370 nm irrespective of the V doping level and the absorption edge is slowly shifts towards lower wavelength (blue shift) [22] are obtained as concentration of V increases. The optical band gap (E_g) values were calculated from the graph obtained using first derivative of transmittance with respect to wavelength ($dT/d\lambda$) and the average wavelength as shown in inset Fig. 4b. From the plots, band gap energy increases as the incorporation of V^{5+} ions into ZnO lattice [23]. Generally, the blue shift indicates the improvement of carrier density due to Moss-Burstein effect [24]. This incorporation of V^{5+} into Zn^{2+} sites does not creates free charge carriers, but increases the charge density. The reason for blue shift is due to difference in ionic radii of V^{5+} and Zn^{2+} and increases the defects in lattice of ZnO which causes broadening of E_g [25]. It is also observed that the dopent V is more active than Zn over the oxygen and hence creates more oxygen vacancies in the surface of the samples [26].

Photoluminescence studies: Fig. 5 shows the photoluminescence spectra of V doped ZnO thin films. Strong peaks (NBA) at 380 nm are obtained, which is due to the transmission of the valence electrons from valence band to conduction band [27]. The intensity of NBA peak increases from undoped to 4 at% of V doped ZnO and decreases for 6 at%. The shift towards lower wavelength (blue shift) was observed in NBA peak up to 4 at% and red shift for 6 at% of vanadium concentration. It proves that the carrier concentration of ZnO:V increases up to 4 at% and the decreased for 6 at %. A weak peak at 424 was due to the zinc interstitials recombination of electrons and holes in the conduction band, which supports the shift of absorption edge towards lower wavelength in optical transmission spectra. 467nm peak represents the oxygen vacancy on the surface of the samples [28].

In all cases, intensity of 467 nm increases as V doping percentage increases from 0 to 4 at % and decreases for 6 at%. That indicates incorporation of V^{5+} ions into Zn^{2+} sites and creates large number acceptor sits over the grain boundaries up to 4 at%. On further increase of V over ZnO lattice, reorientation of Zn^{2+} occurs large in number results reduction of carrier concentration and reduces the acceptor sits on grain boundaries [29].

Surface morphology: HRSEM images of undoped and V doped ZnO samples deposited in glass substrate are shown in Fig. 6. The images show that the grain formation depends on the doping concentrations of V in ZnO lattice. Undoped ZnO sample shows the hexagonal grain of 150 nm and few are very large in size and few nm thickness (Fig. 6a). Moreover the grains are closely packed with porosity and due to the addition of V into ZnO lattice grain size decreases and large quantity of hexagonal plates were around the 2 at% and 4 at% samples (Fig. 6b-c). The sizes of the grains were around 50 to 100 nm and on further increase in concentration creates agglomeration and hexagonal plates merges together to form clusters (Fig. 6d, 6 at%). Porosity nature is increases from undoped to 6 at% of V:ZnO. This HRSEM images are compatible with that of XRD and optical studies.

The elemental composition conforms the presence of vanadium, zinc and oxygen on the surface of 4 at% of V:ZnO sample (Fig. 6e). For undoped sample, it is observed that the surface is smooth and has large peaks of height around 120 nm (Fig. 6f), due to addition of V into ZnO the average roughness (Ra) and Root mean value of roughness are decreases from 0.039 μm to 18 nm and 0.195 μm to 83 nm, respectively for undoped to doped 4 at% of V (Fig. 6h), whereas 6 at% sample has average roughness (Ra) of 29.76 nm and Root mean value is 97 nm (Fig. 6i). From the above values, it is observed that 4 at% has the better result than the other sample. Above range of values are suitable for active attraction of oxygen from air and suitable for gas sensing study.

Magnetic, electrical and figure of merit: The M-H curve (Fig. 7a) shows that the pure and vanadium doped ZnO thin films behaves like paramagnetic material at room temperature with the applied field ranging from -15 kG to 15 kG. The paramagnetic property increases from undoped to 4 at% of vanadium doped ZnO sample. On further increases in vanadium paramagnetic property decreases, this is due to the strong exchange of interaction between the oxygen vacancy and uncompensated spin distributed over the film [30]. Incorporation of V^{5+} ions creates local holes concentration in ZnO lattice and enhances

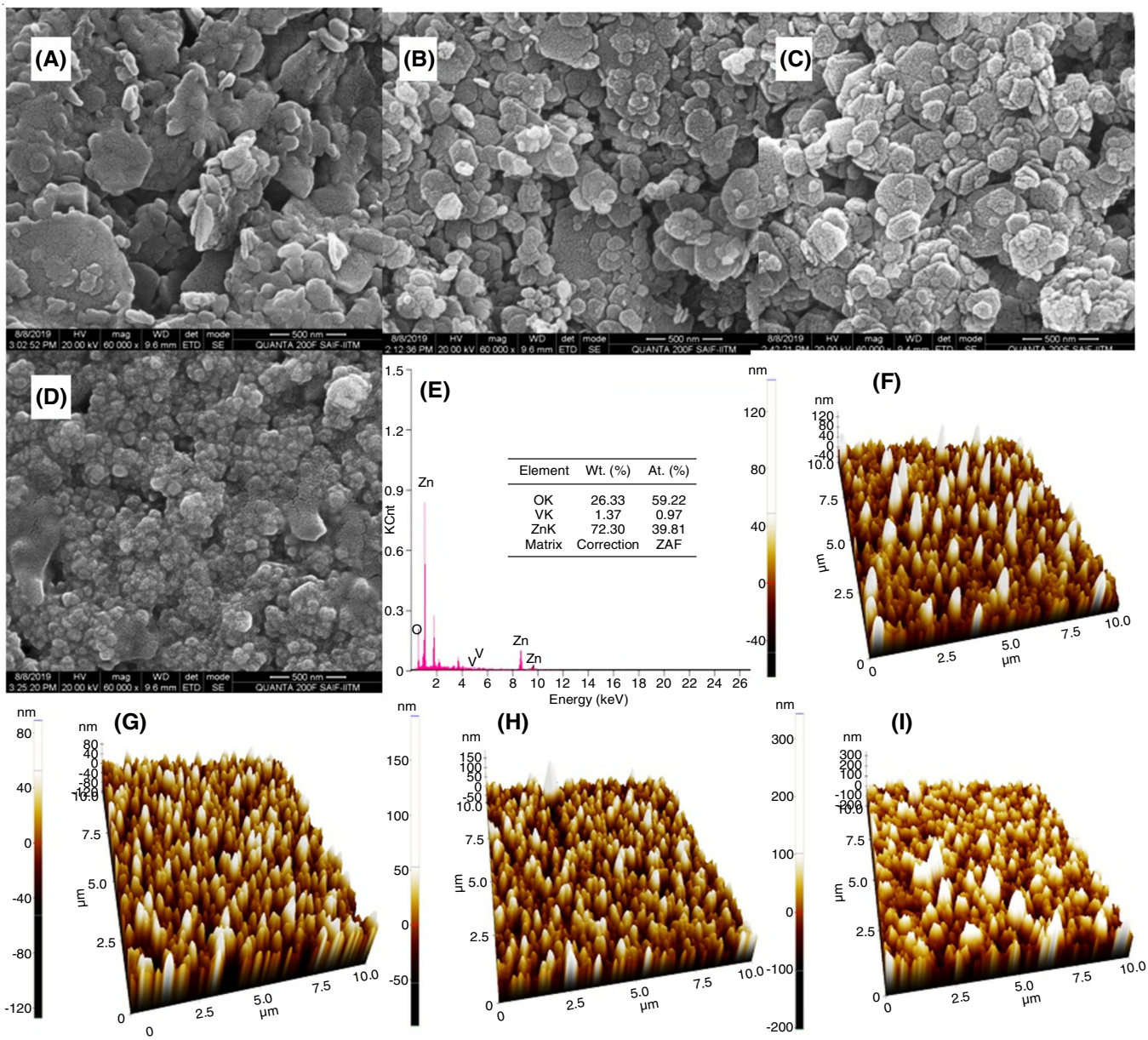

Fig. 6. HRSEM images of (A) 0, (B) 2, (C) 4 and (D) 6 at% vanadium doped zinc oxide samples, (E) EDAX of 4 at% V:ZnO sample and AFM images of (F) 0, (G) 2, (H) 4 and (I) 6 at% V:ZnO samples

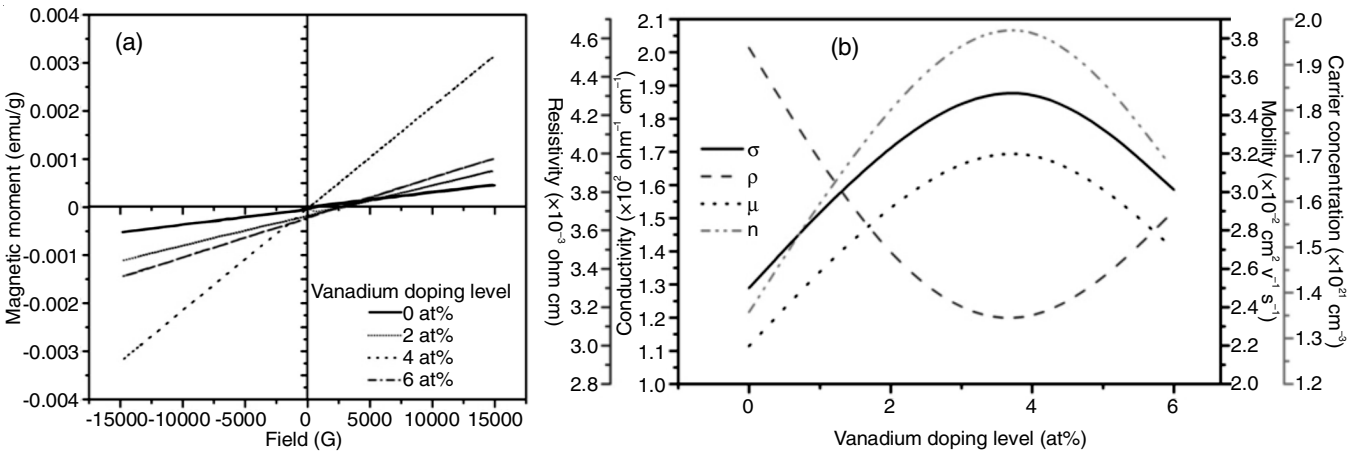

Fig. 7. (a) M-H curve at room temperature for undoped and vanadium doped ZnO samples (b) the change of electrical resistivity, mobility, carrier concentration and Conductivity with respect to vanadium doping level of ZnO thin film samples

large number of global acceptor concentration [31]. As paramagnetic property increases, its coercivity (H_c) and retentivity (M_r) are decrease remarkably and its values are listed in Table-2. The 4 at% V:ZnO shows low saturated magnetization (M_s) compared to other samples has very low magnetization. Such low magnetization materials are used for drug delivery systems and as optical windows in optoelectronic devices.

TABLE-2
MAGNETIC PARAMETERS OF
UNDOPED AND V:ZnO SAMPLES

Sample (at%)	Coercivity (H_c) Gauss	Magnetization (M_s) × 10^{-3} emu	Retentivity (M_r) × 10^{-6} emu
0	113.45	49.6	7.06
2	17.54	42.5	6.57
4	56.69	12.4	4.68
6	18.24	31.9	5.14

Fig. 7b shows the change in electrical parameters like mobility, resistivity, carrier concentration and sheet resistance by Hall effect measurement. The change in sheet resistance and value of optical band gap listed in Table-3. It is observed that the resistivity decreases for undoped to V doped ZnO and there is an increase of conductivity and mobility. The undoped sample has the highest resistivity 4.55 × 10^{-3} Ω cm due to air chemisorptions of oxygen on the surface of the film. This absorbed that oxygen act as a barrier and causes high resistivity [32].

TABLE-3
OPTICAL BANDGAP, SHEET RESISTANCE AND
QUALITY FACTOR OF UNDOPED AND V:ZnO SAMPLES

Sample (at%)	Optical bandgap E_g (eV)	Sheet resistance × 10^2 R_{sh} Ω/^{2}	Transmittance at 550 nm (%)	Quality factor (ϕ) × 10^{-6} (Ω/^{2})$^{-1}$
0	3.259	91.0	87.35	28.45
2	3.264	67.0	89.09	47.01
4	3.267	59.7	88.34	48.64
6	3.257	74.0	87.35	34.98

The V:ZnO shows the resistivity decreases to 3.35 × 10^{-3} Ω cm and 2.98 × 10^{-3} Ω cm for 2 at% and 4 at%, respectively. This is due to substitution of V^{5+} on Zn^{2+} sites in the ZnO lattice. The resistivity increases on further doping and this due to the occupancy of some vanadium ions into interstitial sites ZnO lattice which gives more electrons for conductions. Higher doping of V (6 at%) causes reorientation of ZnO and increases crystalline size and interstitial sites decreases. This resulted an increase of resistance on higher level of vanadium in ZnO [33]. The figure of merit represents the quality factor of transparent conducting oxide sample and it is calculated using Haacke's formula [34]. From the calculation 4 at% of V:ZnO sample shows maximum value as given in Table-3.

Resistance *vs.* light intensity: Fig. 8 shows a change in resistance concerning light intensity. 1 cm^2 area of the sample was connected to electrodes through silver paste and placed in sample holder. When sample exposed to light and change in resistance with respect to light intensity was recorded in the graph. From Fig. 8, it is observed that the resistance of the

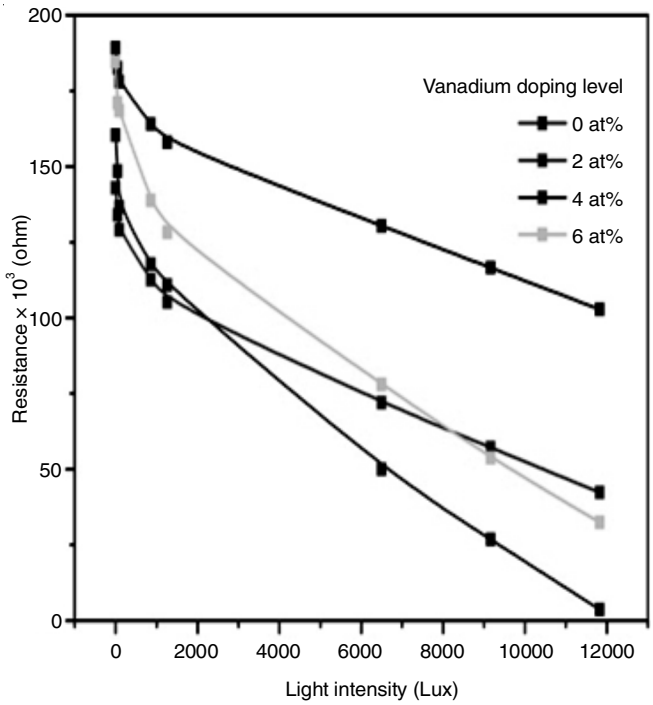

Fig. 8. Effect of resistance towards intensity of light for V:ZnO samples

samples slowly decreases and reaches minimum at 1,20,000 Lux. Undoped sample has highest resistance and its rate of change in resistance is low, when it is compared to other samples. Rate of change in resistance for all the samples between 1,000 Lux to 1,20,000 Lux is very high as compared to low range of Lux. The rate of change of resistance of sample 4 at% is higher than the other samples and this is due to a large number of ionized oxygen vacancies, on the surface of the film as discussed in photoluminescence study. The sample with V 6 at%, shows low rate of change of resistance and this is due to lack of ionized oxygen vacancy on the surface of the sample.

Conclusion

In present study, the effect of vanadium on physical properties of ZnO samples was investigated. Magnetic study shows the enhancement of paramagnetic property due to the addition of vanadium. Hall effect shows the remarkable improvement in carrier concentration, resistivity and mobility. The sheet resistance decreases to 59.5 × 10^2 Ω/^{2} for 4 at% of vanadium. All the samples achieved the transmittance above 80% in the visible region after the addition of vanadium. From the XRD pattern, the addition of vanadium did not alter the single phase hexagonal wurtzite structure in the film. The performances of the samples on light intensity study shows doping of vanadium enhance the rate of decreases in resistance is high when compared to other undoped sample. From all the study, it is concluded that vanadium doped ZnO are the promising material for the optoelectronic and paramagnetic applications.

CONFLICT OF INTEREST

The authors declare that there is no conflict of interests regarding the publication of this article.

REFERENCES

1. W. Liu and H. Wang, *J. Materiomics*, **6**, 385 (2020); https://doi.org/10.1016/j.jmat.2019.12.006
2. C.T. Pan, Y.C. Chen, C.C. Hsieh, C.H. Lin, C.Y. Su, C.K. Yen, Z.H. Liu and W.C. Wang, *Sens. Actuators A Phys.*, **216**, 318 (2014); https://doi.org/10.1016/j.sna.2014.05.024
3. Y. Liu, Y. Li and H. Zeng, *J. Nanomater.*, **2013**, 196521 (2013); https://doi.org/10.1155/2013/196521
4. T. Maruyama and J. Shionoya, *J. Mater. Sci. Lett.*, **11**, 170 (1992); https://doi.org/10.1007/BF00724682
5. M. Thirumoorthi and J.T.J. Prakash, *Mater. Sci. Eng. B*, **248**, 114402 (2019); https://doi.org/10.1016/j.mseb.2019.114402
6. A. Smaali, S. Abdelli-Messaci, S. Lafane, A. Mavlonov, J. Lenzner, S. Richter, M. Kechouane, O. Nemraoui and K. Ellmer, *Thin Solid Films*, **700**, 137892 (2020); https://doi.org/10.1016/j.tsf.2020.137892
7. B.G. Shohany and A.K. Zak, *Ceram. Int.*, **46**, 5507 (2020); https://doi.org/10.1016/j.ceramint.2019.11.051
8. A. Renitta and K. Vijayalakshmi, *Sens. Actuators B Chem.*, **237**, 912 (2016); https://doi.org/10.1016/j.snb.2016.07.017
9. C.M. Mahajan and M.G. Takwale, *J. Alloys Compd.*, **584**, 128 (2014); https://doi.org/10.1016/j.jallcom.2013.08.136
10. Z.N. Kayani, H. Nazli, S. Kousar, S. Riaz and S. Naseem, *Ceram. Int.*, **46**, 14605 (2020); https://doi.org/10.1016/j.ceramint.2020.02.261
11. K. Ravichandran, E. Sindhuja, R. Uma and T. Arun, *Surf. Eng.*, **33**, 512 (2017); https://doi.org/10.1080/02670844.2016.1270797
12. D.-H. Xia, J. Wang, Z. Qin, Z. Gao, Z. Wu, J. Wang, L. Yang, W. Hu and J.-L. Luo, *Mater. Chem. Phys.*, **233**, 133 (2019); https://doi.org/10.1016/j.matchemphys.2019.05.056
13. A. Jaworek and A.T. Sobczyk, *J. Electrost.*, **66**, 197 (2008); https://doi.org/10.1016/j.elstat.2007.10.001
14. K. Ravichandran, K. Subha, N. Dineshbabu and A. Manivasaham, *J. Alloys Compd.*, **656**, 332 (2016); https://doi.org/10.1016/j.jallcom.2015.09.115
15. Q. Fan, D. Li, J. Li and C. Wang, *J. Alloys Compd.*, **829**, 154483 (2020); https://doi.org/10.1016/j.jallcom.2020.154483
16. K. Ravichandran, M. Vasanthi, K. Thirumurugan, K. Karthika and B. Sakthivel, *J. Mater. Sci. Mater. Electron.*, **26**, 5451 (2015); https://doi.org/10.1007/s10854-015-3101-5
17. T. Prasada Rao, M.C. Santhosh Kumar, A. Safarulla, V. Ganesan, S.R. Barman and C. Sanjeeviraja, *Physica B*, **405**, 2226 (2010); https://doi.org/10.1016/j.physb.2010.02.016
18. F.Z. Bedia, A. Bedia, N. Maloufi, M. Aillerie, F. Genty and B. Benyoucef, *J. Alloys Compd.*, **616**, 312 (2014); https://doi.org/10.1016/j.jallcom.2014.07.086
19. A.S.H. Hameed, C. Karthikeyan, S. Sasikumar, V. Senthil Kumar, S Kumaresan and G. Ravi, *J. Mater. Chem. B*, **1**, 5950 (2013); https://doi.org/10.1039/C3TB21068E
20. Y. Wang, Z.J. Peng, Q. Wang and X.L. Fu, *Surf. Eng.*, **33**, 217 (2017); https://doi.org/10.1080/02670844.2016.1212519
21. R. Mimouni, K. Boubaker and M. Amlouk, *J. Alloys Compd.*, **624**, 189 (2015); https://doi.org/10.1016/j.jallcom.2014.11.016
22. R. Mariappan, V. Ponnuswamy, A. Chandra Bose, A. Chithambararaj, R. Suresh and M. Ragavendar, *Superlatt. Microstruct.*, **65**, 184 (2014); https://doi.org/10.1016/j.spmi.2013.10.005
23. T. Suzuki, H. Chiba, T. Kawashima and K. Washio, *Thin Solid Films*, **605**, 53 (2016); https://doi.org/10.1016/j.tsf.2015.11.064
24. M. Al-Hashem, S. Akbar and P. Morris, *Sens. Actuators B Chem.*, **301**, 126845 (2019); https://doi.org/10.1016/j.snb.2019.126845
25. A. Paulson, N.A.M. Sabeer and P.P. Pradyumnan, *Mater. Sci. Eng. B*, **262**, 114745 (2020); https://doi.org/10.1016/j.mseb.2020.114745
26. N. Al-Hardan, M.J. Abdullah and A.A. Aziz, *Appl. Surf. Sci.*, **257**, 8993 (2011); https://doi.org/10.1016/j.apsusc.2011.05.078
27. V. Srivastava and K. Jain, *RSC Adv.*, **5**, 56993 (2015); https://doi.org/10.1039/C5RA11050E
28. C. Cachoncinlle, C. Hebert, J. Perriere, M. Nistor, A. Petit and E. Millon, *Appl. Surf. Sci.*, **336**, 103 (2015); https://doi.org/10.1016/j.apsusc.2014.09.186
29. O. Gurbuz and M. Okutan, *Appl. Surf. Sci.*, **387**, 1211 (2016); https://doi.org/10.1016/j.apsusc.2016.06.114
30. R.K. Upadhyay and L.A. Kumaraswamidhas, *Surf. Eng.*, **32**, 289 (2016); https://doi.org/10.1179/1743294415Y.0000000109
31. A. Goktas, I.H. Mutlu and Y. Yamada, *Superlatt. Microstruct.*, **57**, 139 (2013); https://doi.org/10.1016/j.spmi.2013.02.010
32. G. Shanmuganathan and I.B. Shameem Banu, *Superlatt. Microstruct.*, **75**, 879 (2014); https://doi.org/10.1016/j.spmi.2014.08.024
33. S. Ghosh, G.G. Khan, A. Ghosh, S. Varma and K. Mandal, *CrystEngComm*, **15**, 7748 (2013); https://doi.org/10.1039/c3ce40717a
34. M. Fitta, H. Prima-Garcia, P. Czaja, T. Korzeniak, M. Krupinski, M. Wojtyniak and M. Ba³anda, *RSC Adv.*, **7**, 1382 (2017); https://doi.org/10.1039/C6RA25775E